TDP1 facilitates chromosomal single-strand break repair in neurons and is neuroprotective *in vivo*

Sachin Katyal[1,4], Sherif F El-Khamisy[2,3,4],
Helen R Russell[1], Yang Li[1], Limei Ju[2],
Keith W Caldecott[2,*] and
Peter J McKinnon[1,*]

[1]Department Genetics and Tumor Cell Biology, St Jude Children's Research Hospital, Memphis, TN, USA, [2]Genome Damage and Stability Center, University of Sussex, Falmer, Brighton, UK and [3]Biochemistry Department, Faculty of Pharmacy, Ain Shams University, Cairo, Egypt

Defective Tyrosyl-DNA phosphodiesterase 1 (TDP1) can cause spinocerebellar ataxia with axonal neuropathy (SCAN1), a neurodegenerative syndrome associated with marked cerebellar atrophy and peripheral neuropathy. Although SCAN1 lymphoblastoid cells show pronounced defects in the repair of chromosomal single-strand breaks (SSBs), it is unknown if this DNA repair activity is important for neurons or for preventing neurodegeneration. Therefore, we generated $Tdp1^{-/-}$ mice to assess the role of Tdp1 in the nervous system. Using both *in vitro* and *in vivo* assays, we found that cerebellar neurons or primary astrocytes derived from $Tdp1^{-/-}$ mice display an inability to rapidly repair DNA SSBs associated with Top1–DNA complexes or oxidative damage. Moreover, loss of Tdp1 resulted in age-dependent and progressive cerebellar atrophy. $Tdp1^{-/-}$ mice treated with topotecan, a drug that increases levels of Top1–DNA complexes, also demonstrated significant loss of intestinal and hematopoietic progenitor cells. These data indicate that TDP1 is required for neural homeostasis, and reveal a widespread requisite for TDP1 function in response to acutely elevated levels of Top1-associated DNA strand breaks.

Introduction

DNA repair involves specific enzymes that address a multitude of different types of DNA lesions (Barnes and Lindahl, 2004; Wood *et al*, 2005). Tyrosyl-DNA phosphodiesterase 1 (TDP1) is involved in the repair of DNA strand breaks associated with a variety of DNA termini, the best characterized of which are Topoisomerase-1 (Top1)-associated 3′-termini arising from abortive Top1–DNA complexes (Yang *et al*, 1996; Inamdar *et al*, 2002; Liu *et al*, 2002; Zhou *et al*, 2005; Interthal *et al*, 2005a; Nitiss *et al*, 2006). Top1 relieves torsional stress in DNA via formation of a transient intermediate known as the cleavage complex, whereby Top1 forms a covalent phosphodiester bond between an active site tyrosyl residue and the 3′-end of a DNA nick (Wang, 2002; Pommier *et al*, 2003). TDP1 cleaves the tyrosyl–DNA bond in Top1-associated strand breaks, thereby removing Top1 peptide from the 3′-terminus and enabling repair of the DNA strand breaks (Pouliot *et al*, 1999; Wood *et al*, 2005; Interthal *et al*, 2005a). Although Top1-cleavage complexes are normally very short lived, they can be converted into Top1-linked single-strand breaks (SSBs) or double-strand breaks (DSBs) by collision with the transcription or DNA replication machinery (Avemann *et al*, 1988; Holm *et al*, 1989; Hsiang *et al*, 1989; Kroeger and Rowe, 1989; Bendixen *et al*, 1990; Ryan *et al*, 1991; Wu and Liu, 1997; Strumberg *et al*, 2000). Treatment with the Top1 inhibitor camptothecin (CPT), increases the half-life of cleavage complexes and therefore the likelihood of their conversion into Top1-associated SSBs and DSBs. This property of CPT and related compounds make them valuable as anticancer agents (Rodriguez-Galindo *et al*, 2000).

Homozygous mutation of *TDP1* can cause spinocerebellar ataxia with axonal neuropathy (SCAN1), an autosomal recessive neurodegenerative syndrome (Takashima *et al*, 2002). SCAN1 individuals present with ataxia associated with marked cerebellar atrophy, peripheral neuropathy and distal muscle weakness. However, substantial defects outside of the nervous system have not been reported, and TDP1-deficiency appears to selectively affect terminally differentiated neurons. To date, elucidation of the cellular role of TDP1 in mammalian cells has relied primarily on lymphoblastoid cell lines derived from SCAN1 (Plo *et al*, 2003; El-Khamisy *et al*, 2005; Zhou *et al*, 2005; Interthal *et al*, 2005a, b; Miao *et al*, 2006). However, the rarity of SCAN1 and a lack of suitable animal models have precluded detailed studies that specifically address the role of TDP1 in the mammalian nervous system or elsewhere.

Consequently, we have generated $Tdp1^{-/-}$ mice and employed both *in vitro* and *in vivo* assays to demonstrate that primary neural cells, including cerebellar granule neurons, derived from these animals display SCAN1-like DNA repair deficiencies, characterized by a failure to repair DNA SSBs associated with abortive Top1 activity and oxidative damage. Moreover, we show that loss of TDP1 results in progressive age-related cerebellar atrophy. Finally, we show that topotecan-induced increases in the level of Top1-associated DNA strand breaks leads to loss of progenitor cells in the intestine and to hematopoietic defects, thereby revealing important roles fulfilled by TDP1 *in vivo* beyond those evident from the pathology of SCAN1.

*Corresponding authors. KW Caldecott, Genome Damage and Stability Center, University of Sussex, Falmer, Brighton BN1 9RQ, UK.
Tel.: +44 1323 877519; Fax: +44 1323 678121;
E-mail: k.w.caldecott@sussex.ac.uk or PJ McKinnon, Department Genetics and Tumor Cell Biology, St Jude Children's Research Hospital, 332 North Lauderdale, Memphis, TN 38105, USA. Tel.: +1 901 495 2700; Fax: +1 901 526 2907; E-mail: peter.mckinnon@stjude.org
[4]These authors contributed equally to this work

Results

Generation of Tdp1-deficient mice

A targeted ES cell line was obtained from BayGenomics in which a gene trap insertion strategy using a β-*Geo* cassette caused an interruption in the *Tdp1* locus (Figure 1A). ES cells containing the mutant *Tdp1* allele were used to generate $Tdp1^{+/-}$ mice that were intercrossed to produce $Tdp1^{-/-}$ mice, which were born at the expected Mendelian ratios, were fertile and had a normal life expectancy. Additionally, no signs of premature aging, such as graying hair, or any age-related issues with general ambulation or well-being (e.g. piloerection of the fur) were observed. Analysis of the mutant *Tdp1* transcript by RT–PCR confirmed a truncated *Tdp1* message resulting from termination of transcription from the β-*Geo* cassette at nucleotide 1369 (aa 456) of *Tdp1* (Genbank accession no. NM_028354) (Figure 1B). The resulting transcript lacks a large portion of the Tdp1 primary coding sequence, including the active site histidine that is mutated in SCAN1 (His493). Western blot analysis failed to detect Tdp1 in tissues isolated from $Tdp1^{-/-}$ mice, whereas a single band of ∼67 kDa was detected in tissues from $Tdp1^{+/+}$ mice, thereby indicating that the mutant transcript likely encodes an unstable polypeptide (Figure 1C). Loss of Tdp1 did not affect Top1 levels (Figure 1C). We conclude from these data that the *Tdp1* mutation does not produce functional Tdp1 protein.

Defective DNA single-strand break repair in primary $Tdp1^{-/-}$ neural cells

It has been proposed that TDP1-dependent SSB repair (SSBR) is required for genetic integrity in neurons (El-Khamisy *et al*,

2005; El-Khamisy and Caldecott, 2007). To test this, we employed primary cortical astrocytes and post-mitotic cerebellar granule neurons isolated from wild-type (WT; $Tdp1^{+/+}$) and $Tdp1^{-/-}$ mice. The astrocytes were immuno-positive for the astrocyte marker GFAP (glial fibrillary acidic protein) (Figure 2A), and the post-mitotic granule neurons were immunopositive for neuron-specific markers and for the cell-cycle inhibitor protein p27^{KIP1} (Figure 2B and data not shown). The $Tdp1^{-/-}$ astrocytes proliferated at a similar rate to WT controls, and did not show any enhanced cytogenetic abnormalities as judged by spectral karyotype analysis (data not shown). However, for the purpose of measuring SSBR, these cells were rendered quiescent by allowing them to reach confluence. Pulse-labelling with BrdU confirmed that <5% of astrocytes were proliferating under these conditions (data not shown).

We next used the alkaline comet assay to compare the induction and repair of SSBs in quiescent astrocytes and in cerebellar post-mitotic neurons following treatment with CPT, H_2O_2, and γ-rays. Although alkaline comet analysis measures both SSBs and DSBs, the vast majority (>95%) of breaks induced by these agents (particularly in noncycling cells) are SSBs and so this assay primarily measures rates of SSBR (Bradley and Kohn, 1979; Hsiang *et al*, 1985; Prise *et al*, 1989; Ismail *et al*, 2005). Strikingly, whereas primary cortical astrocytes and cerebellar neurons from WT mice maintained very low levels of DNA strand breaks throughout a 1hr incubation with CPT, a genotoxin that induces abortive SSB intermediates of Top1 activity (Hsiang *et al*, 1985), high levels of DNA strand breakage accumulated in primary astrocytes and cerebellar neurons from $Tdp1^{-/-}$ mice (Figure 2C and D). Based on previous studies with SCAN1 lymphoblastoid
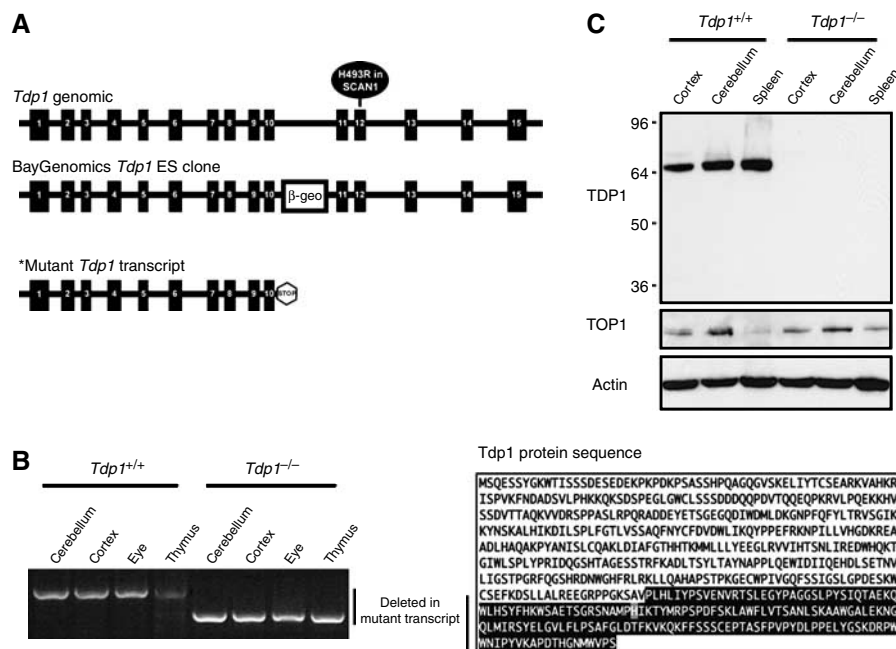

Figure 1 Generation of $Tdp1^{-/-}$ mice. (**A**) Schematic of the murine *Tdp1* gene and associated mutant transcript after a β-geo cassette insertion in intron 10–11, that results in a premature stop after exon 10. (**B**) $Tdp1^{-/-}$ tissues show a shorter transcript due to termination by β-geo. The amino-acid sequence deleted in the mutant $Tdp1^{-/-}$ transcript is shaded in black. The active site histidine-493 (mutated in SCAN1) is also lost in the Tdp1 mutant. (**C**) Western blot analysis of Tdp1 in tissues from $Tdp1^{+/+}$ and $Tdp1^{-/-}$ mice did not detect protein in any $Tdp1^{-/-}$ tissue. Top1 levels were similar between $Tdp1^{+/+}$ and $Tdp1^{-/-}$ tissues.
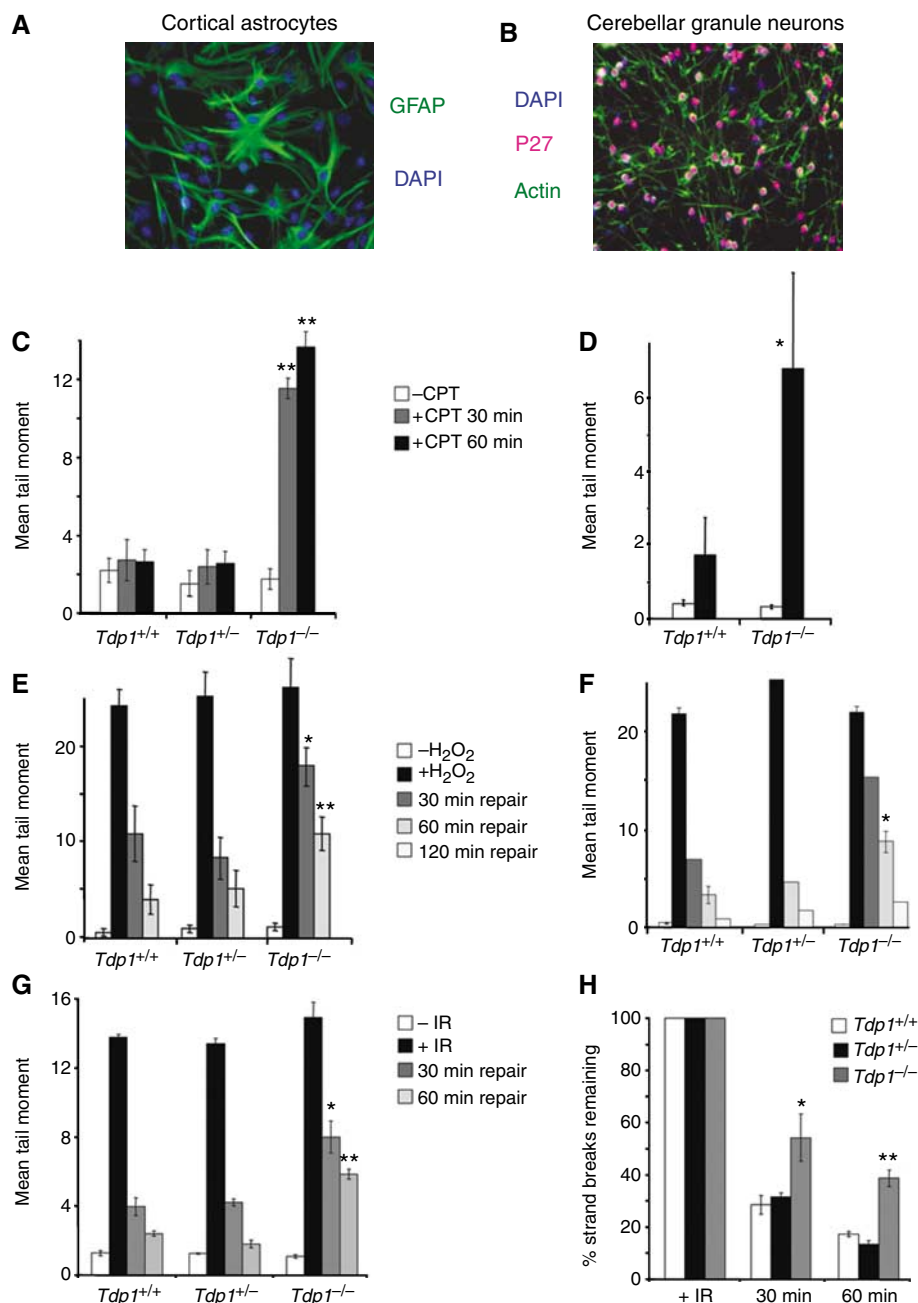
Figure 2 Defective DNA strand break repair in primary cortical astroctyes and cerebellar granule cells (neurons) from $Tdp1^{-/-}$ mice. (**A**) Astrocytes were immunostained for GFAP (green) and counterstained with DAPI (blue). (**B**) Cerebellar granule cells were immunostained for p27^{KIP1} (red) and actin (green), and counterstained with DAPI (blue). (**C, D**) Astrocytes (C) and cerebellar granule cells (D) from $Tdp1^{+/+}$, $Tdp1^{+/-}$, or $Tdp1^{-/-}$ mice were incubated in the absence or presence of 14 μM CPT for the indicated periods and DNA strand breakage then quantified by alkaline comet assays. (**E, F**) Astrocytes (E) and cerebellar granule cells (F) from $Tdp1^{+/+}$, $Tdp1^{+/-}$ or $Tdp1^{-/-}$ mice were mock-treated ($-H_2O_2$) or treated ($+H_2O_2$) with H_2O_2 and then incubated for the indicated repair periods in drug-free medium. DNA strand breakage was quantified by alkaline comet assays. (**G**) Astrocytes were treated with γ-radiation (20 Gy) and then incubated for the indicated repair periods. DNA strand breaks were quantified at the indicated times by alkaline comet assays. (**H**) The data in (G) was plotted as the mean fraction of DNA strand breaks remaining (±s.e.m.) at the indicated time points. Asterisks denote statistically significant (*$P<0.05$; **$P<0.005$; *t*-test) differences between $Tdp1^{-/-}$ and $Tdp1^{+/+}$ histograms at the indicated time points. Mean tail moments were quantified for at least 50 cells/sample/experiment and data are the average of at least three independent experiments (±s.e.m.).

cell lines (El-Khamisy *et al*, 2005), the difference in average tail moments equates to 5000–10 000 extra total strand breaks in $Tdp1^{-/-}$ compared to WT cells and results from defective SSBR, rather than a difference in levels of DNA damage induction.

As oxidative stress is an etiological factor in a variety of neurodegenerative diseases and in human ageing, we deter-mined whether Tdp1-dependent SSBR is also required in primary neural cells to repair DNA strand breaks induced by H_2O_2, a physiologically relevant oxidizing agent, and ionizing radiation (IR). Although these agents primarily in-duce DNA strand breaks with 3′-phosphate and 3′-phospho-glycolate termini, DNA strand breaks or base lesions can induce Top1-associated DNA strand breaks indirectly, by

stabilizing nearby Top1 cleavage complexes (Pourquier *et al*, 1997, 1999; Christiansen and Westergaard, 1999; Lesher *et al*, 2002). In addition, TDP1 can process 3′-phosphoglycolate termini present at DSBs (Inamdar *et al*, 2002; Zhou *et al*, 2005). While similar levels of DNA strand breakage were induced by H_2O_2 in WT and $Tdp1^{-/-}$ quiescent primary astrocytes and granule cells, the rate at which these breaks declined during post-treatment incubations in drug-free media was significantly reduced in the $Tdp1^{-/-}$ astrocytes and neurons (Figure 2E and F). Similar results were observed following IR (Figure 2G and H). Together, these data demonstrate that Tdp1 is required in primary neural cells for the rapid repair both of DNA SSBs induced by CPT and for a subset of such breaks induced by H_2O_2, and IR.

Absence of a measurable defect in DNA DSB repair in $Tdp1^{-/-}$ neural cells

To directly examine whether $Tdp1^{-/-}$ neural cells also possess a defect in DSBR, we compared quiescent $Tdp1^{+/+}$ and $Tdp1^{-/-}$ astrocytes for formation of γ-H2AX foci, an established marker for DSBs (Rogakou *et al*, 1998), following treatment with H_2O_2, CPT and IR. We observed a small difference in the number and intensity of γ-H2AX foci that accumulated in $Tdp1^{-/-}$ astrocytes following a 30 min incubation with CPT, compared to WT astrocytes (Figure 3A). However, the difference in DSBs between the two cell types, as measured by foci number, was less than five per cell, and thus did not contribute significantly to the extra 5000-10 000 total DNA strand breaks that accumulated in $Tdp1^{-/-}$ astro-

cytes under these experimental conditions. Moreover, the rate at which these foci declined during post-treatment incubations was similar in $Tdp1^{+/+}$ and $Tdp1^{-/-}$ cells (Figure 3A).

We similarly did not observe any measurable difference in the appearance or kinetics of removal of γ-H2AX foci in $Tdp1^{+/+}$ or $Tdp1^{-/-}$ astrocytes following oxidative stress induced by H_2O_2 or γ-rays (Figure 3B and C). Note that in these experiments, post-treatment incubation for ~30 min was required for γ-H2AX to be detected. In both cases, the rate at which γ-H2AX foci declined during post-treatment incubation was similar in $Tdp1^{+/+}$ and $Tdp1^{-/-}$ neural cells, with γ-H2AX foci returning to near-background levels within 6–24 h. A similar outcome was found using Rad51 immunocytochemistry to examine DNA DSB repair via homologous recombination, in which radiation-induced Rad51 foci recovery was indistinguishable between WT and $Tdp1^{-/-}$ astrocytes (data not shown). In summary, although $Tdp1^{-/-}$ primary neural cells exhibit a profound defect in the repair of SSBs, we failed to detect a measurable defect in DSBR in these cells.

$Tdp1^{-/-}$ neural cells are deficient in the repair of Top1-associated SSBs in vitro

We next examined whether we could recapitulate the SSBR defect observed in quiescent $Tdp1^{-/-}$ primary astrocytes, using an 18-mer oligonucleotide that harbors a phosphotyrosine-linked 3′-terminus. This is a substrate for TDP1 and mimics the type of protein-linked 3′-terminus present at abortive Top1 cleavage complexes induced by CPT. We first
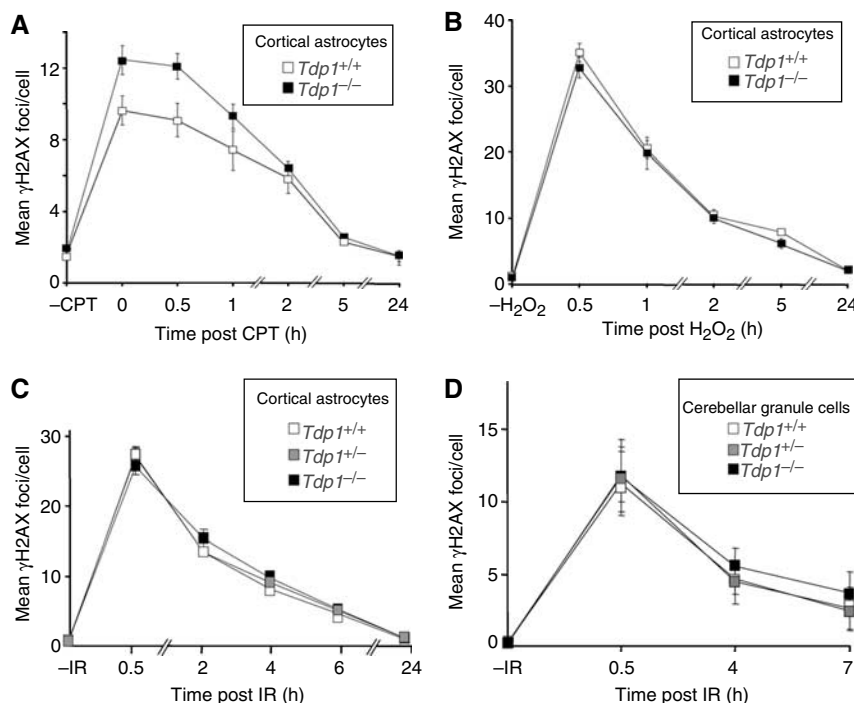

Figure 3 DNA DSB repair in $Tdp1^{-/-}$ neural cells. (**A**) The mean number of γ-H2AX foci was quantified in quiescent primary astrocytes mock-treated (−CPT) or treated (+CPT) with 14 μM CPT and then incubated for the indicated repair period in drug-free medium. (**B**) The mean number of γ-H2AX foci was quantified in quiescent primary astrocytes mock-treated (−H_2O_2) or treated with H_2O_2 and then incubated for the indicated repair period in drug-free medium. (**C**, **D**) The mean number of γ-H2AX foci was quantified in quiescent primary astrocytes (C) or cerebellar granule cells (D) from $Tdp1^{+/+}$, $Tdp1^{+/-}$ or $Tdp1^{-/-}$ mice that were mock-irradiated (−IR) or were γ-irradiated (3 Gy) and then incubated for the indicated repair periods. Data are the mean number of foci/cell calculated from 50 cells/sample and are the mean of at least three independent experiments (±s.e.m.).

compared cell extracts from quiescent $Tdp1^{+/+}$ and $Tdp1^{-/-}$ astrocytes for their ability to remove tyrosine from the 3′-end of the single-stranded oligonucleotide. Whereas significant removal of the 3′-Y was observed in reactions containing as little as 0.16 μg of total protein from $Tdp1^{+/+}$ extracts (Figure 4A, lane 9), none of the 3′-Y was removed by $Tdp1^{-/-}$ astrocyte extracts, even at the highest protein concentration (20 μg/reaction) employed (Figure 4A, compare lanes 3 and 4). However, addition of recombinant human TDP1 to $Tdp1^{-/-}$ astrocyte extracts restored the ability to remove 3′-Y (Figure 4A, lane 2). As the cerebellum is the most affected organ in SCAN1 patients and in $Tdp1^{-/-}$ mice (see later), we next examined total protein extracts prepared from the whole cerebellum from 1- or 5-month-old mice for the ability to remove tyrosine from the 3′ end of the single-stranded oligonucleotide. Complete removal of the 3′-Y was observed in reactions containing $Tdp1^{+/+}$ cerebellar extracts, whereas $Tdp1^{-/-}$ extracts failed to remove the 3′-Y (Figure 4B, compare lanes 2 and 3, and 4 and 6). Again, the

defect in $Tdp1^{-/-}$ extract was complemented by addition of recombinant human TDP1 (Figure 4B, lane 7). Next, we assembled the tyrosine-linked oligonucleotide into a duplex substrate containing a SSB with a tyrosine residue linked covalently at the 3′-terminus (see cartoon in Figure 4C and D, right), which reflects the type of break upon which TDP1 might operate *in vivo*. This repair reaction requires removal of the tyrosine by TDP1 followed by removal of the resulting 3′-phosphate by PNK, and ligation of the remaining nick by a DNA ligase such as XRCC1/DNA ligase IIIα. WT, but not $Tdp1^{-/-}$ astrocytes (Figure 4C) or cerebellar extract (Figure 4D) converted labelled 18-mer into labelled 43-mer repair product, confirming the requirement for TDP1 to repair SSBs with protein-linked 3′-termini (Figure 4C; left panel and Figure 4D, lanes 2 and 3). These defects in $Tdp1^{-/-}$ protein extracts were again complemented by addition of recombinant human TDP1 (Figure 4C; right panel and Figure 4D, lanes 4–7). Thus, the defect in SSBR observed in primary neural cells is also evident *in vitro*, in SSBR reactions
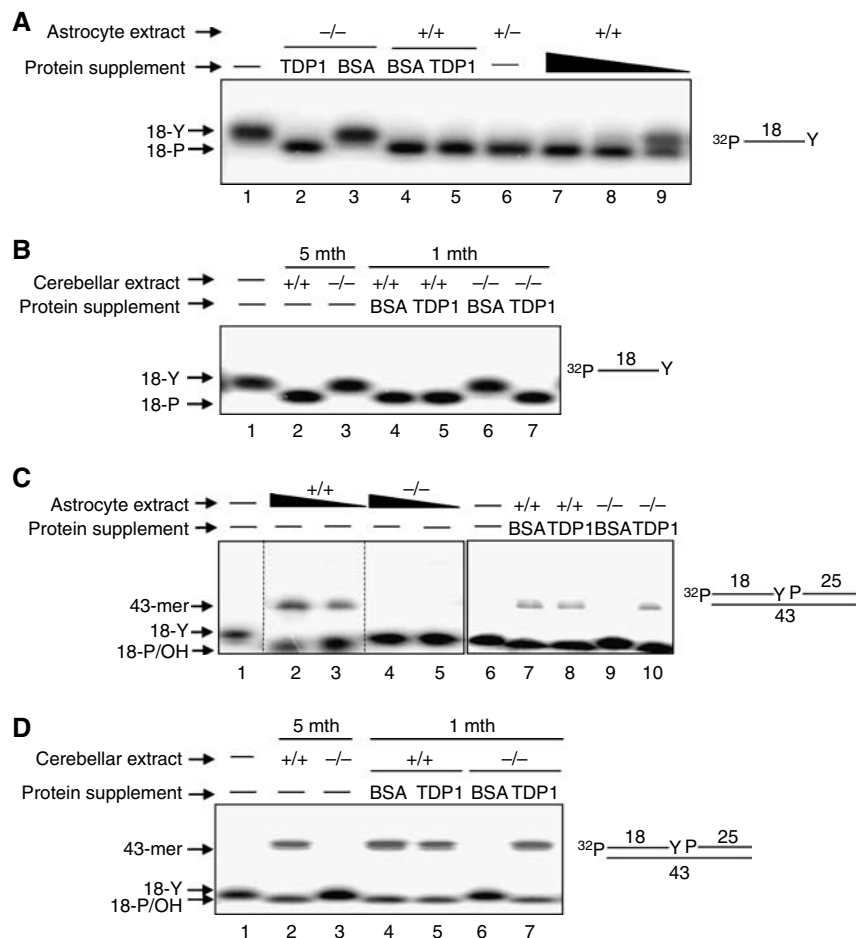

Figure 4 A SSB repair defect in quiescent primary astrocyte and cerebellar extracts from $Tdp1^{-/-}$ mice. (**A**) Cell extract (20 μg total protein in lanes 2–6 and 4, 0.8, and 0.16 μg total protein in lanes 7, 8, and 9, respectively) from quiescent primary cortical astrocytes of the indicated genotype were incubated with radiolabelled 18-mer-Y oligonucleotide (right) for 60 min at 37°C and reaction products fractionated by denaturing PAGE. (**B**) As in (A), except that reactions employed protein extract (50 μg total protein) from a whole-cerebellum from 1-month-old (1 month) or 5-month-old (5 months) mice. Where indicated, reactions were supplemented with 14 nM of BSA or recombinant human TDP1. (**C**) Cell extract (10 μg total protein in lanes 3 and 5; 20 μg total protein in lanes 2 and 4) from primary cortical astrocytes of the indicated genotype were incubated with radiolabelled oligonucleotide duplex harboring a SSB with a 3′-Y terminus (right) for 60 min at 37°C and reaction products fractionated by denaturing PAGE. Where indicated, reactions were supplemented with 14 nM of BSA or recombinant human TDP1. (**D**) As in (C), except that reactions employed protein extract (50 μg total protein) from a whole-cerebellum from 1-month-old (1 month) or 5-month-old (5 months) mice. Reaction products were visualized by autoradiography.

reconstituted with protein extract from quiescent cortical astrocytes or whole cerebellum.

Reduced cerebellar size in Tdp1$^{-/-}$ mice

A comparison of age-matched WT and $Tdp1^{-/-}$ mice revealed a marked reduction in cerebral and cerebellar size in the mutant animals (Figure 5A). Whole-brains isolated from 17-month-old $Tdp1^{-/-}$ showed a 10% reduction in gross brain mass when compared and corrected for body mass differences to WT littermate controls. As a primary CNS tissue affected in SCAN1 is the cerebellum, we measured and compared the cerebellar to brain ratio (C:B) of $Tdp1^{+/+}$ and $Tdp1^{-/-}$ mice. Morphometric analysis of $Tdp1^{-/-}$ mice revealed a progressive age-dependent reduction in $Tdp1^{-/-}$ C:B compared to that of $Tdp1^{+/+}$ (Figure 5A and B). Although little difference is seen in young (2 months old)

mice, analysis of 7, 13, and 17 months old mouse brains demonstrated a gradual reduction (6, 10, and 15%, respectively) in $Tdp1^{-/-}$ cerebellar size when compared to age-matched $Tdp1^{+/+}$ cerebella. However, $Tdp1^{-/-}$ cerebellar morphology and foliation was indistinguishable from $Tdp1^{+/+}$, as judged by cellular cytoarchitecture and analysis of differentiation markers that identify a variety of cerebellar cell types (Figure 5C). These data suggest that loss of TDP1 results in gradual age-related cerebellar atrophy, characteristic of SCAN1.

Tdp1$^{-/-}$ mice have hypoalbuminemia

Two extraneurological features of SCAN1 are hypoalbuminemia and hypercholesterolemia (Takashima *et al*, 2002). SCAN1 patients have albumin levels below the levels typical of normal individuals (range of 3.6–4.8 g/dl) and elevated
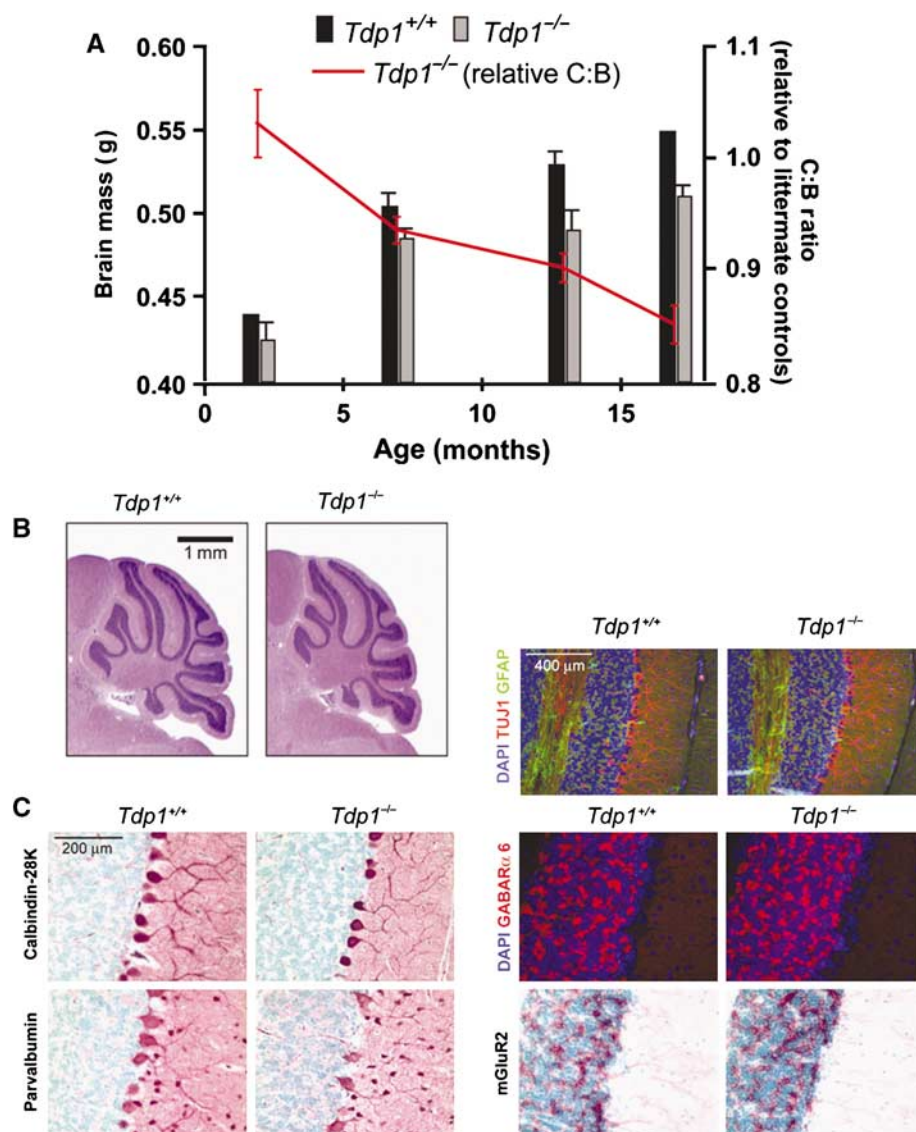

Figure 5 Neuropathology of $Tdp1^{-/-}$ mice. (**A**) Comparison of average brain mass and cerebellar size in 2, 7, 13, and 17 months old $Tdp1^{+/+}$ and $Tdp1^{-/-}$ mice. Average C:B from $Tdp1^{-/-}$ brain were compared as a proportion of C:B from $Tdp1^{+/+}$ littermates and corrected for body weight differences. (**B**) Hematoxylin and eosin staining of 17-month-old $Tdp1^{+/+}$ and $Tdp1^{-/-}$ cerebellum sections highlighting the reduced cerebellar size observed in mutant mice. (**C**) Immunohistochemical analysis of cerebellar cell types: Tuj1 (neurons), GFAP (glia), GABA receptor alpha-6 (mature granule cell neurons), mGluR2 (Golgi cells), calbindin-28K (Purkinje cells), and parvalbumin (Purkinje cells and interneurons). Tuj1/GFAP fluorescent micrographs are at ×200 magnification, while all other sections are shown at ×400 magnification.

cholesterol levels at or above the higher limit of levels typical of normal individuals (range of 129–224 mg/dl). Consequently, we analyzed blood serum samples from $Tdp1^{+/+}$ and $Tdp1^{-/-}$ mice for these features. Serum albumin levels of $Tdp1^{-/-}$ mice from a variety of ages (6–17 months) were considerably reduced (mean of 2.1 g/dl, $n = 12$), falling well below the normal typical range (2.6–4.6 g/dl), whereas levels from WT mice were within the normal range (mean of 2.7 g/dl, $n = 8$). However, analysis of cholesterol levels revealed no differences between WT and mutant mice. These data, combined with our finding of cerebellar atrophy, show that $Tdp1^{-/-}$ mice have both neurological and extraneurological similarities to SCAN1 individuals.

$Tdp1^{-/-}$ mice are hypersensitive to Topotecan

To examine whether genotoxic insult *in vivo* can affect $Tdp1^{-/-}$ tissue, we determined the effect of increasing the level of Top1-associated DNA damage in $Tdp1^{+/+}$ and $Tdp1^{-/-}$ mice by treatment with the Top1 inhibitor and CPT analogue, topotecan (TPT). Sex-matched WT and mutant littermates at 1 month of age were treated with six daily doses of 1 mg/kg TPT via intraperitoneal injection, and total weight gain/loss was assessed 24 h after each injection. Saline-injected $Tdp1^{+/+}$, $Tdp1^{-/-}$, and TPT-injected WT mice showed positive weight gain profiles throughout the treatment period, whereas TPT-injected $Tdp1^{-/-}$ mice showed a profound sensitivity to the drug, ending the treatment-period with substantial weight loss (Figure 6A and B).

Increased sensitivity of proliferating intestinal cells to topotecan in $Tdp1^{-/-}$ mice

TPT treatment had a marked effect upon specific organs in the $Tdp1^{-/-}$ mice, including the intestine, thymus, spleen, and bone marrow. While the intestine is a tissue susceptible to genotoxic agents (Booth and Potten, 2000), the response of the $Tdp1^{-/-}$ mice to TPT was unusually severe. TPT-treatment of the $Tdp1^{-/-}$ intestine resulted in disorganization and reduction in numbers of PCNA-positive cells in the lower crypt compared to similarly treated WT controls (Figure 6C, left and middle panels). We used phospho-PTEN^{S380} to confirm that TPT affected intestinal progenitor cells in the $Tdp1^{-/-}$ gut (Figure 6C, right panels, arrowheads). In contrast, intestinal goblet cells were largely unaffected by TPT, but showed increased cell clustering upon drug-dependent intestinal cell loss in the $Tdp1^{-/-}$ gut (Figure 6C, red arrowheads). We also found a pronounced effect upon the brain after systemic application of TPT in $Tdp1^{-/-}$ mice. We reasoned that this neural effect of TPT could result from systemic effects such as nutritional absorption issues and dehydration, and that with time after drug removal we would also see a relative correction in brain weight. After a 1-week recovery from TPT to allow for intestinal cell repopulation, we found a marked gain in body weight and a significant recovery in brain weight and size in $Tdp1^{-/-}$ suggesting that the effects of TPT on the brain are secondary to profound systemic effects (not shown).

Increased sensitivity of hematopoietic cells to topotecan in $Tdp1^{-/-}$ mice

We also analyzed hematopoietic cells after TPT treatment, as these are known to be susceptible to DNA damage. We found

a substantial size reduction in $Tdp1^{-/-}$ spleen and thymus after TPT compared to WT mice (Figures 6D and E). This marked effect in the TPT-treated $Tdp1^{-/-}$ thymus was associated with a near total loss of $CD4^+CD8^+$ immature T-cells (Figure 7A; 0.8%). The remaining $CD4^+CD8^+$ double-positive thymocytes were undergoing apoptosis and were positive for annexin V (Figure 7A; lower right panel). In mock-treated $Tdp1^{-/-}$ or TPT-treated WT mice, $CD4^+CD8^+$ thymocyte profiles were indistinguishable and showed no increased apoptosis. In contrast, mature thymocytes ($CD4^+CD8^-CD3^+$ and $CD4^-CD8^+CD3^+$) were present at similar levels in mock-treated $Tdp1^{-/-}$ and TPT-treated $Tdp1^{+/+}$ and $Tdp1^{-/-}$ mice. However, there were increased numbers of mature $Tdp1^{-/-}$ thymocytes undergoing apoptosis compared to $Tdp1^{+/+}$ in response to TPT treatment (Figure 7A). These data indicate that TPT-treatment of the $Tdp1^{-/-}$ thymus markedly affects T-cell development and perturbs progression of thymopoiesis with immature ($CD4^+CD8^+$) T-cells in particular and maturing $Tdp1^{-/-}$ T-cells being sensitive to Top1-mediated DNA damage.

Bone marrow cells are sensitive to TPT (Aydemir and Bilaloglu, 2003) and accordingly both WT and KO mice displayed marked genotoxicity after TPT treatment. However, bone marrow from TPT-treated $Tdp1^{-/-}$ mice revealed a two-fold reduction in $B220^{low+}CD43^-$ pre-mature B cells (Figure 7C, 3.0%) compared to that of $Tdp1^{+/+}$ bone marrow (Figure 7C, 5.7%). Similarly, there were more $B220^{+low}CD43^-$ annexin V-positive cells in TPT-treated $Tdp1^{-/-}$ marrow compared to TPT-treated $Tdp1^{+/+}$ marrow (Figure 7C, middle right panel). Additionally, marrow cells from TPT-treated $Tdp1^{-/-}$ mice showed a substantial loss in $c\text{-}Kit^+$ hematopoietic progenitor cells, whereas TPT-treated $Tdp1^{+/+}$ mice and mock-treated mice remained unaffected. These data indicate that $Tdp1^{-/-}$ marrow stem cells and progenitors show enhanced sensitivity to Top1-mediated DNA damage. Thus, loss of TDP1 function affects specific hematopoietic cell types suggesting a role for TDP1 after DNA damage at specific stages during hematopoiesis.

Discussion

TDP1 participates in the repair of DNA SSBs and mutation of TDP1 leads to the neurodegenerative syndrome SCAN1. It has been suggested that this syndrome occurs because TDP1 is important for repair of DNA SSBs in neurons that might otherwise inhibit transcription (El-Khamisy et al, 2005, 2007; Miao et al, 2006). However, the rarity of the disease and the unavailability of SCAN1 neuronal tissue have restricted earlier studies to the use of immortalized SCAN1 lymphoblastoid cells. Therefore, to directly assess the physiological role of TDP1, we generated mice with germline inactivation of $Tdp1$. We found a pronounced defect in the repair of chromosomal SSBs arising from CPT, oxidative stress or IR in neurons. We also observed an age-related cerebellar atrophy in $Tdp1^{-/-}$ mice akin to that observed in individuals with SCAN1 (Takashima et al, 2002). These data support defective repair of DNA SSBs in the nervous system as an etiological agent for SCAN1, strengthening the link between DNA damage, and SSBs in particular, and neurodegeneration (Rolig and McKinnon, 2000; El-Khamisy et al, 2005).

In contrast to SSBs, we failed to detect a significant defect in the repair of DSBs in $Tdp1^{-/-}$ neural cells after CPT, H_2O_2,
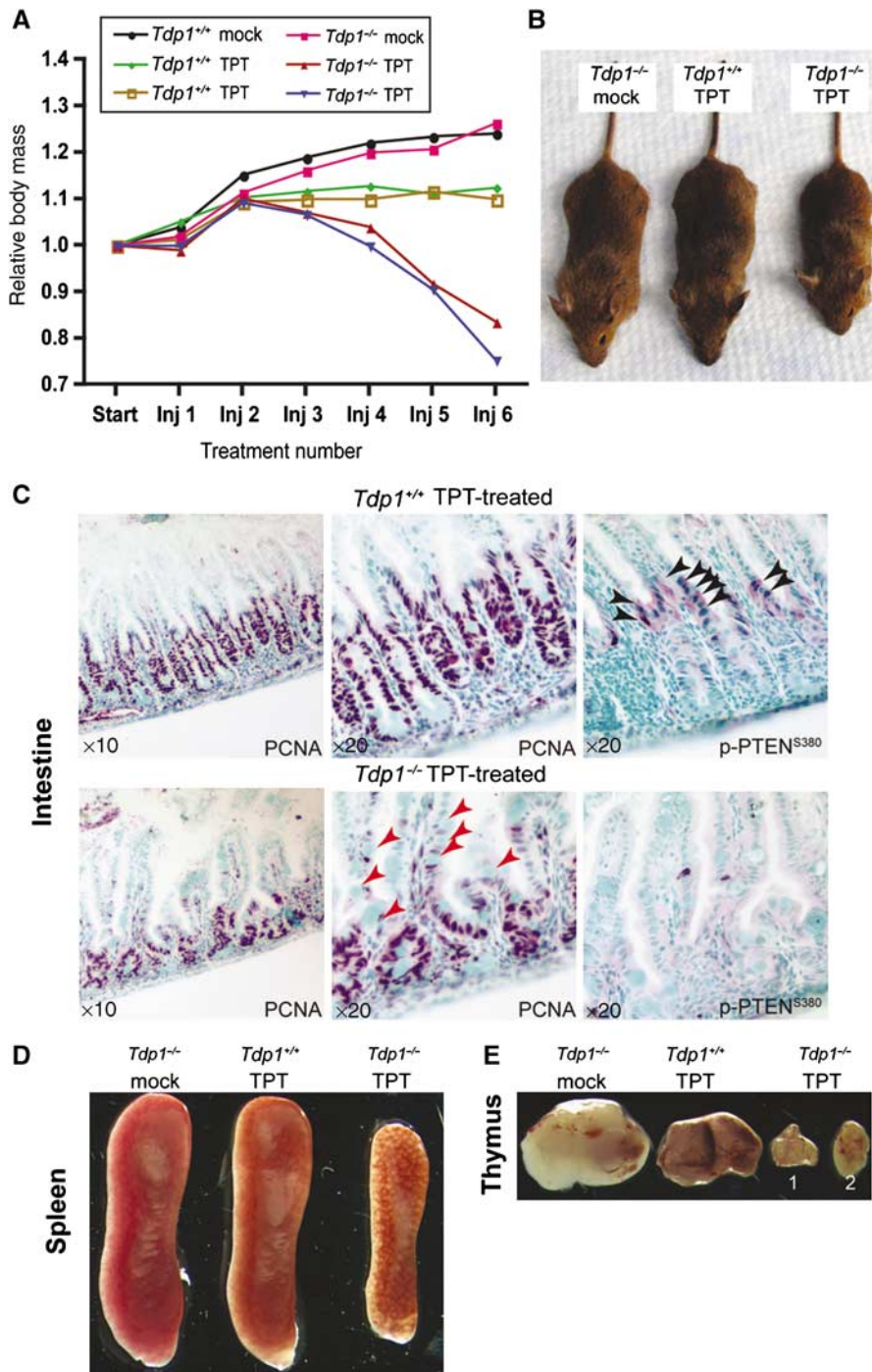
Figure 6 Sensitivity of $Tdp1^{-/-}$ mice to Topotecan. (**A**) Body weight profiles of mock- and TPT-treated $Tdp1^{+/+}$ and $Tdp1^{-/-}$ mice over drug treatment period. One-month-old mice were weighed daily before six topotecan doses (1 mg/kg/day) administered over an 8-day period. Weight profiles were plotted relative to the starting weight of each mouse. (**B**) $Tdp1^{+/+}$ and $Tdp1^{-/-}$ mice after mock (left) and topotecan treatment (center and right). (**C**) Immunohistochemical analysis of $Tdp1^{+/+}$ and $Tdp1^{-/-}$ intestine after TPT treatment. Intestinal sections were immunolabelled with anti-PCNA (proliferative cells) or anti-phospho-PTEN^{S380} (progenitor cells) antibodies. (**D, E**) Representative murine $Tdp1^{+/+}$ and $Tdp1^{-/-}$ spleen (D) and thymus (E) after mock- and TPT-treatment (six daily IP doses of TPT at 1 mg/kg/day). (E) 1 and 2 denote two independent TPT-treated Tdp1$^{-/-}$ mouse thymus samples.

or IR. These results are in agreement with our previous findings, employing SCAN1 lymphoblastoid cells (El-Khamisy *et al*, 2005). Although we cannot rule out a subtle defect in DSBR, our data are consistent with a defect in SSBR accounting for the phenotypes in SCAN1 or $Tdp1^{-/-}$ mice.

Importantly, we observed a progressive decrease in cerebellar size in $Tdp1^{-/-}$ mice, consistent with an age-depen-

dent cerebellar atrophy akin to that observed in SCAN1. In contrast, however, $Tdp1^{-/-}$ mice lack any obvious ataxic phenotype. Compared to the neuropathology evident in the human *TDP1*-associated disease, the subtler phenotype described here for the mouse model may reflect differences in the specific Tdp1 mutations involved. Alternatively, as SCAN1 is a relatively late-onset (13–15 yr) spinocerebellar
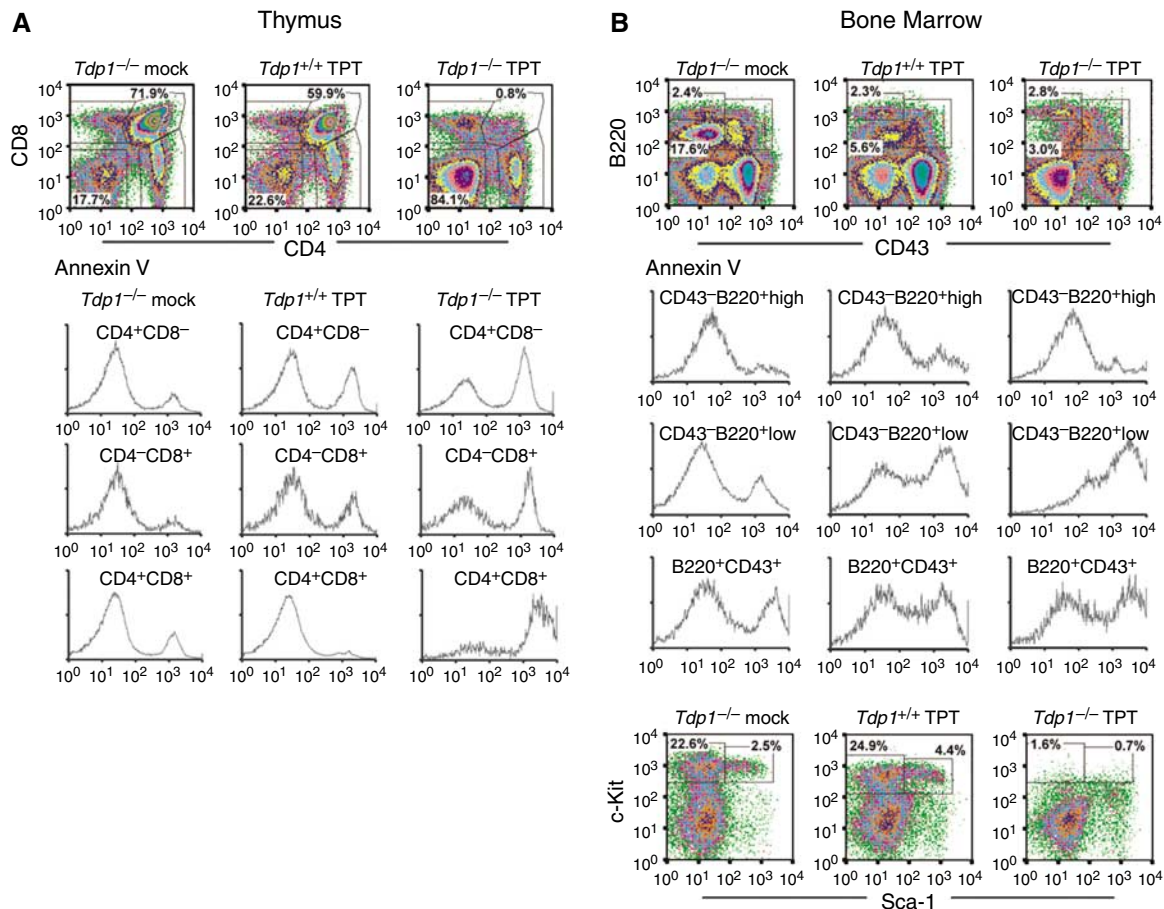
Figure 7 Immunophenotyping of topotecan-treated $Tdp1^{-/-}$ hematopoietic tissue. Dissociated thymus or bone marrow were immunolabelled with fluorescent antibody markers or immunolabelled with annexin V before flow cytometric analysis and the same number of cell events were sorted and analyzed. (**A**) CD4/CD8 analysis of the murine thymus. (**B**) B220/CD43 and c-Kit/Sca-1 analyses of murine bone marrow cells. Percentages on flow panels represent the proportion of cells with the respective immunostaining.

ataxia (Takashima *et al*, 2002), the relatively short life-span of mice (~ 2 yr) may limit the impact of Tdp1 loss in mice to a more subtle decline in neurological function. Consistent with this, preliminary behavioral analyses suggest an age-dependent reduction in neuromuscular control and motor coordination in $Tdp1^{-/-}$ mice (SF El-Khamisy and KW Caldecott, unpublished data). Although SCAN1 is essentially a neurological disease, hypercholesterolemia and hypoalbuminemia are also observed (Takashima *et al*, 2002). Interestingly, hypoalbuminemia was also observed in the $Tdp1^{-/-}$ mice, although the molecular basis for this phenotype remains to be determined. Recently, inactivation of the *Drosophila glaikit* (a TDP1 orthologue) resulted in developmental abnormalities involving loss of cell polarity and epidermal cell death (Dunlop *et al*, 2004). However, as this phenotype results from disruption of localization of membrane proteins, then glaikit inactivation is probably unrelated to SCAN1.

We observed a pronounced sensitivity of various $Tdp1^{-/-}$ tissues to topotecan, including the immune system and the intestine. The immature CD4$^+$CD8$^+$ T-cells in the $Tdp1^{-/-}$ thymus were hypersensitive to TPT treatment and other cell populations, including mature T-cells, underwent enhanced apoptosis. While normal thymopoiesis involves differentiation of immature CD4$^+$CD8$^+$ cells and associated rearrangement of T-cell receptors, a process dependent upon nonhomologous end-joining (Bassing *et al*, 2002), it is likely

that Tdp1 is involved in repairing DNA SSB lesions that arise during normal cellular proliferation. $Tdp1^{-/-}$ B-cells were also very sensitive to genotoxic stress from TPT treatment. Normal B-cell development involves differentiation of hematopoietic stem cells into B220$^{+\,low}$CD43$^+$ progenitors (pro-B) (Hardy and Hayakawa, 2001). Expression and rearrangement of IgH genes allows pro-B cells to differentiate into B220$^{+\,low}$/ CD43$^-$ precursors (pre-B) followed by increasing B220 (immature B) levels and Ig light chain gene rearrangement and expression (B220$^{+\,high}$CD43$^-$IgM$^+$, mature B). In $Tdp1^{-/-}$ bone marrow, most progenitor cells, including c-Kit$^+$ and B220$^{+\,low}$CD43$^-$ cells, were hypersensitive to TPT treatment. In the remaining maturing B cells, there is a substantial loss of B cell precursors upon TPT treatment of $Tdp1^{-/-}$ mice, whereas remaining pre-B cells show increased susceptibility to apoptosis. Similar to the immune system, we also found that $Tdp1^{-/-}$ intestinal progenitor cells were hypersensitive to TPT. Our data therefore demonstrate a previously unrecognized role for TDP1 in responding to acute increases in the level of Top1-associated DNA strand breakage, particularly in progenitor cells of the immune system and the intestine. We previously suggested that the absence of any apparent abnormalities in proliferating cells in this disease reflects, in part, the availability of alternative DNA repair processes, such as homologous recombination, at physiologically relevant levels of SSBs at least (El-Khamisy *et al*, 2005). In light of

our current data, we suggest that such pathways may become saturated in the presence of acutely elevated levels of DNA strand breakage, such as that induced by topotecan, thereby revealing a phenotype in proliferating cells that lack Tdp1. Notably, Nivens *et al* (2004) have showed that retrovirus-mediated overexpression of TDP1 in proliferating bone marrow progenitor cells protects against the cytotoxic effects of Top1 inhibition by CPT.

In summary, we have shown here that TDP1 is critical for DNA SSB repair in primary neural cells and is required to prevent progressive cerebellar atrophy. Together, our data provide direct evidence that chromosomal SSB repair is critical for genetic and neuronal integrity *in vivo*, and reveal previously unrecognized requirements for Tdp1 during exogenous genotoxic stress.

Materials and methods

Generation of Tdp1$^{-/-}$ mice

A Bay Genomics (http://baygenomics.ucsf.edu) ES clone (XD105), containing a β-Geo cassette inserted into intron 10–11 of *Tdp1*, was injected into 3.5-day C57BL/6 blastocysts and transferred to pseudopregnant mothers. Chimeric males were crossed with C57BL/6 females to produce *Tdp1*$^{+/-}$ mice. Germline transmission of the mutation was verified by Southern blot analysis of tail DNA. We confirmed the presence of the *Tdp1* mutation using PCR with primers: 5-TCTTCCAGTTCTTAGCCTCCTCTGC-3′ (Tdp1F), 5-TGG CCTGGATCTCACTCTGGAGGC-3′ (Tdp1R), and 5-GAGTTCCCAG GAGGAGCCAAGGC-3′ (Geo R3). PCR conditions were: 94°C for 30 s, 60°C for 1 min, and 72°C for 1 min, for 35 cycles resulting in a ~250 bp WT PCR product (generated using Tdp1F-Tdp1R primers) and a ~500 bp PCR product (generated with Tdp1F-Geo R3) for the mutant allele. All *Tdp1*$^{+/-}$ animals were maintained on an outbred mixed 129Ola and C57BL/6 background. The SJCRH institutional animal care and use committee approved all animal procedures.

RT–PCR

Total RNA was extracted from postnatal mouse tissues using Trizol reagent (Life Technologies) and 5 μg total RNA was reverse transcribed using oligo(dT)$_{12-18}$ primers and Superscript II (Life Technologies), according to the supplier's protocol. PCR amplification of *Tdp1* WT and mutant cDNA was performed using a forward primer, 5′-CTCGTCGACGTCCCAAGAAAGCAGCTACG-3′ (Sal I restriction site underlined) and a reverse primers 5′- GAATGCGGCCGC AATCCTCACCACGCTAAGCC-3′ (Not I restriction site underlined). PCR conditions were 94°C for 30 s, 60°C for 1 min, and 68°C for 1 min, for 40 cycles. Amplified cDNAs were cloned into the SalI/NotI sites of pcDNA3.1 and sequenced.

Protein extraction and Western blot analysis

Tissues from 1-month-old mice were resuspended in 500 μl of lysis buffer (100 mM Tris–HCl, 150 mM NaCl, pH 7.5, 0.5% SDS, 0.5% NP-40, 0.5% sodium deoxycholate, 1 mM EGTA, 0.5 mM ZnCl$_2$, 0.02% NaN$_3$, 10% Glycerol, 0.1% β-mercaptoethanol, 0.2 mg/ml PMSF and Complete protease inhibitor cocktail (Roche)) and dissociated by passage through a 23G needle. Protein concentrations of whole-cell extracts were quantified using Bradford reagent (Bio-Rad). Proteins (50 μg/lane) were separated through an 8%-SDS poly-acrylamide gel and transferred onto nitrocellulose membrane (Bio-Rad). Blots were immunostained with mouse polyclonal antiserum directed against full-length TDP1 (1:1000; AbNova) followed by horseradish peroxidase-conjugated goat anti-mouse secondary antibody (1:2000; GE Healthcare) and detected using ECL Plus chemiluminescence reagent (GE Healthcare). To assess TOP1 protein levels, immunoblots were stained with mouse anti-Top1 antibody (1:1000; Abcam) and processed as above. Immunostaining with goat polyclonal anti-actin (1:500; Santa Cruz Biotech) antibody served as a protein-loading control.

Immunofluorescence and immunohistochemistry

Tissues were fixed in 4% paraformaldehyde (PFA), and either cryoprotected in 25% PBS-buffered sucrose solution and embedded in O.C.T. (Tissue-Tek) or paraffin embedded. Antigen retrieval was used for all immunohistochemistry and immunofluorescence. For immunohistochemistry, intestinal cryosections were incubated with either mouse anti-PCNA (1:500, Santa Cruz) or rabbit anti-phospho–PTEN^{S380} antibodies (1:500, Cell Signaling) and, brain cryosections were incubated with either rabbit anti-mGluR2 (1:500, Upstate), mouse anti-calbindin-D-28-K (1:500, Sigma), or mouse anti-parvalbumin (1:500, Chemicon) overnight at room temperature after quenching endogenous peroxidase with 0.6% hydrogen peroxide in methanol. Immunoreactivity was visualized with a vasoactive intestinal peptide substrate kit (V.I.P.; Vector Labs) according to the manufacturer's directions after tissues were treated with biotinylated secondary antibody and avidin DH-biotinylated horseradish peroxidase-H complex (Vectastain Elite kit; Vector Labs). Sections were counterstained with 0.1% methyl green (Vector Labs), dehydrated, and mounted in DPX reagent. For immunofluorescence, brain cryosections were blocked for 1 h in 5% goat serum/1% BSA and then incubated with mouse anti-β-tubulin III (Tuj1, 1:500; BAbCo), rabbit anti-GFAP (1:250; AbCam), or rabbit anti-GABARα6 (1:500, Chemicon), overnight at room temperature. Sections were subsequently immunolabelled with Cy3-conjugated goat anti-mouse (1:400; Jackson Immunoresearch) and/or FITC-conjugated goat anti-rabbit secondary antibodies (1:200; Molecular Probes) and mounted with Vectashield anti-fade reagent containing DAPI (Vectorlabs). Images were captured using an Axioskop 2.0 fluorescence microscope (Carl Zeiss) and a SPOT camera (Diagnostic Instruments Inc.).

For fluorescent labelling of cortical astrocytes and cerebellar granule neurons, cells were grown on glass coverslips, fixed with 4% PFA in PBS for 10 min and permeabilized for 5 min in 0.5% Triton X-100/PBS. Cells were immunostained with antibodies diluted in PBS/3% BSA; mouse anti-GFAP (1:1000; Sigma) and anti-p27^{Kip1} (1:500; BD pharmingen), followed by the appropriate Alexa 555- and Alexa 488-conjugated secondary antibodies. For labelling of actin, Alexa 488-conjugated phalloidin was diluted in 3% BSA (1:500; Molecular Probes). For γH2AX analysis, cells were exposed to γ-irradiation (3 Gy) using a cesium-137 source (CammaeII 1000) in complete medium on ice or incubated with 14 μM CPT in serum-free medium for 30 min at 37°C or 70 μM H$_2$O$_2$ in PBS for 10 min on ice. Cells were then incubated in drug-free medium for the indicated time at 37°C, and fixed with 4% PFA/PBS for 10 min at room temperature, followed by incubation with 0.5% Triton X-100/PBS for 5 min on ice. Cells were then rinsed with PBS and incubated with 5% BSA for 30 min at 37°C to block nonspecific binding, followed by incubation with mouse anti-phospho-γH2AX monoclonal antibodies (Upstate; clone JBW301, 1/800 dilution in 3%BSA) for 30 min at 37°C. After rinsing with PBS, cells were incubated in FITC-conjugated anti-mouse IgG (DAKO) secondary antibodies at 1:200 dilution in 4% BSA for 30 min at 37°C. Nuclei were counterstained with 0.000025% DAPI.

Computation of C:B ratio was performed using the ImageJ image analysis software (NIH). Micrographs of matched hematoxylin and eosin mouse brain sections were traced using the freehand tool and the total area bound by the traced region was computed using the measure tool. The C:B ratio was obtained by dividing the measured cerebellar area by the measured area of the entire brain. Each C:B ratio was derived from analysis of three brain sections from three independent *Tdp1*$^{-/-}$ mice and their corresponding littermate controls. The *Tdp1*$^{-/-}$ C:B ratio was plotted relative to the C:B ratio derived from littermate controls after compensating for any body-weight differences by multiplying the relative mutant C:B with the ratio of mutant:WT body weights.

Isolation of primary mouse astrocytes and granule cell neurons

Cerebral cortices from P3 or P4 brains were isolated and dissociated by passage through a 5 ml pipette. Cells were resuspended in a 1:1 mix of Dulbecco's modified Eagle's medium and Ham's nutrient mixture F-12 (DMEM-F12; Gibco-BRL) supplemented with 10% fetal bovine serum, 2 mM L-glutamine, 100 U/ml penicillin, 100 μg/ml streptomycin, and 20 ng/ml epidermal growth factor (Sigma). The primary astrocytes were allowed to establish in Primeria T-25 tissue culture flasks (Falcon) at 37°C in a humidified low oxygen (3 or 5%) incubator. The medium was changed after 4 days and astrocyte monolayers reached confluence 2 days later. The purity of the culture was confirmed by immunofluorescence using an anti-GFAP antibody (Sigma).

Cerebellar granule cells were purified from P6-P8 brains (Hatten, 1985). Cerebellar tissue were treated with trypsin (Gibco)-DNAse I (Worthington) and triturated into a single-cell suspension. The cell suspension was applied to a Percoll gradient (35/60%) and separated by centrifugation. Enriched granule cell neurons were grown in neural basal medium (Gibco) supplemented with 2 mM L-glutamine, 100 U/ml penicillin, 100 µg/ml streptomycin, 2% D + Glucose (Sigma), 1 × SPITE (Sigma), 1 × Oleic acid albumin/linoleic acid (Sigma), and 16 µg/ml N-Acetyl Cysteine (Sigma) on poly-D-lysine-/matrigel-coated (Gibco and Becton Dickson, respectively) glass-bottom multi-chamber slides (Falcon) or glass coverslips at a density of 300 000 cells/well.

Alkaline comet assays

Cells ($\sim 3 \times 10^5$ cells/sample) were treated with either 14 µM CPT for 30–60 min at 37°C, 70 µM (granule cell neurons) or 100 µM (astrocytes) H_2O_2 for 10 min on ice, or γ-irradiation (20 Gy; cesium 137) on ice. Cells were then incubated for the indicated repair periods in drug-free medium at 37°C. Cells were then suspended in pre-chilled PBS and mixed with equal volume of 1.2% low-gelling-temperature agarose (Sigma, type VII) maintained at 42°C. The cell suspension was immediately layered onto pre-chilled frosted glass slides (Fisher) pre-coated with 0.6% agarose and maintained in the dark at 4°C until set, and for all further steps. Slides were immersed in pre-chilled lysis buffer (2.5 M NaCl, 10 mM Tris–HCl, 100 mM EDTA pH 8.0, 1% Triton X-100, 1% DMSO; pH10) for 1 h, washed with pre-chilled distilled water (2×10 min), and placed for 45 min in pre-chilled alkaline electrophoresis buffer (50 mM NaOH, 1 mM EDTA, 1% DMSO). Electrophoresis was then conducted at 25 V (0.6 V/cm) for 25 min, followed by neutralization in 400 mM Tris–HCl pH 7.0 for 1 h. Finally, DNA was stained with Sybr Green I (1:10 000 in PBS) for 30 min. DNA strand breakage was expressed as 'comet tail moment,' which is the product of the tail length and the fraction of DNA that has exited the nucleus during electrophoresis (Olive et al, 1990). The comet tail moment was measured for at least 50 cells/sample using Comet Assay IV software (Perceptive Instruments, UK).

DNA single-strand break repair assay

An 18-mer oligonucleotide (18-Y; 5′-TCCGTTGAAGCCTGCTTT-P-Tyr-3′) containing a 3′ phosphotyrosyl terminus (Yang et al, 1996) was a generous gift from H Nash (National Institute of Mental Health, Bethesda, USA). The 25-mer (5′-GACATACTAACTTGAGC GAAACGGT-3′) and 43-mer (3′-TAGGCAACTTCGGACGAAACTG TATGATTGAACTCGCTTTGCC-5′) oligonucleotides employed to generate a duplex substrate containing a nick with a 3′-phospho-tyrosine terminus. The 18-Y-mer was synthesized by MWG. The 18-Y-mer was phosphorylated by T4 PNK in 25 µl reactions containing 5 µCi [γ-^{32}P] ATP at 7000 Ci/mmol (ICN), and after the removal of unincorporated nucleotides annealed with equimolar amounts of the 25-mer and 43-mer. Soluble cerebellar (50 µg total protein) or quiescent astrocyte cell extract (0.16–20 µg protein) was then mixed with 25 nM substrate (10 µl reaction volume) and incubated at 37°C for 1 h in 25 mM HEPES pH 8, 130 mM KCl, 1 mM DTT, 10 mM MgCl$_2$, and 1 mM ATP. Reactions containing the single-stranded DNA substrate were performed in the absence of MgCl$_2$ to allow TDP1 activity (which is Mg^{2+}-independent) and prevent PNK activity. Where indicated, reactions were supplemented with 14 nM

recombinant human TDP1 or BSA. Reactions were stopped by addition of 1 × loading buffer (44% deionized formamide, 2.25 mM Tris-borate, 0.05 mM EDTA, 0.01% xylene cyanol, 1% bromophenol blue), heated at 90°C for 10 min, and repair products fractionated by denaturing electrophoresis at 250 V, and visualized by autoradiography. For preparation of cerebellum homogenate a single freshly isolated cerebellum of the appropriate genotype was rinsed with PBS and snap frozen in liquid nitrogen. The cerebellar tissue was homogenized while still frozen using a tissue homogenizer. Cerebellar homogenate was then lysed in 20 mM Tris–HCl pH 7.5, 10 mM EDTA, 1 mM EGTA, 100 mM NaCl, 1% Triton X-100, and protease inhibitors for 15 min on ice and soluble cell extract recovered by centrifugation at 10 000 r.p.m. for 5 min at 2°C. For cell extract prepared from cultures of quiescent primary cortical astrocytes, $\sim 3 \times 10^6$ cells were lysed as above. Protein concentrations were determined using a BioRad protein assay kit.

Blood serum analysis

Whole-blood was collected by intraorbital sampling from $Tdp1^{+/+}$ and $Tdp1^{-/-}$ mice between 6 and 17 months of age. Total albumin and cholesterol levels in blood serum were measured using a Vitros DT 60II Chemistry System (Ortho-Clinical Diagnostics, Rochester, NY).

Topotecan administration and flow-cytometric analysis

Topotecan hydrochloride (Hycamtin; Glaxo Smith Kline) was dissolved in 0.9% NaCl and diluted to a concentration of 100 µg/ml. $Tdp1^{+/+}$ and $Tdp1^{-/-}$ sex-matched littermates, 1-month-age, underwent intraperitoneal injection with a volume of 10 µl of either normal saline or Topotecan per gram of body weight (1 mg/kg/day). Mice underwent three daily injections, followed by a 2-day break, followed by another three daily injections, for a total of six injections. The brain and intestine were preserved for sectioning, while the thymus and bone marrow were collected and processed for flow cytometric analysis. Marrow cells were isolated from both murine hindlimbs. All tissues were passed through a 70 µM nylon membrane into PBS + 2% FBS to generate single-cell suspensions. Cells were immunolabelled with the appropriate fluorescently labelled antibodies (BD Biosciences) and analyzed using a Becton Dickinson FACScan flow cytometer (Becton Dickinson Immunocytometry). Data were compiled and analyzed using CellQuest.

Acknowledgements

References

Avemann K, Knippers R, Koller T, Sogo JM (1988) Camptothecin, a specific inhibitor of type I DNA topoisomerase, induces DNA breakage at replication forks. Mol Cell Biol 8: 3026–3034

Aydemir N, Bilaloglu R (2003) Genotoxicity of two anticancer drugs, gemcitabine and topotecan, in mouse bone marrow in vivo. Mutat Res 537: 43–51

Barnes DE, Lindahl T (2004) Repair and genetic consequences of endogenous DNA base damage in mammalian cells. Annu Rev Genet 38: 445–476

Bassing CH, Swat W, Alt FW (2002) The mechanism and regulation of chromosomal V(D)J recombination. Cell 109 (Suppl): S45–S55

Bendixen C, Thomsen B, Alsner J, Westergaard O (1990) Camptothecin-stabilized topoisomerase I-DNA adducts cause premature termination of transcription. Biochemistry 29: 5613–5619

Booth C, Potten CS (2000) Gut instincts: thoughts on intestinal epithelial stem cells. J Clin Invest 105: 1493–1499

Bradley MO, Kohn KW (1979) X-ray induced DNA double strand break production and repair in mammalian cells as measured by neutral filter elution. Nucleic Acids Res 7: 793–804

Christiansen K, Westergaard O (1999) Mapping of eukaryotic DNA topoisomerase I catalyzed cleavage without concomitant religation in the vicinity of DNA structural anomalies. Biochim Biophys Acta 1489: 249–262

Dunlop J, Morin X, Corominas M, Serras F, Tear G (2004) Glaikit is essential for the formation of epithelial polarity and neuronal development. Curr Biol 14: 2039–2045

El-Khamisy SF, Caldecott KW (2007) DNA single-strand break repair and spinocerebellar ataxia with axonal neuropathy-1. Neuroscience 145: 1260–1266

El-Khamisy SF, Hartsuiker E, Caldecott KW (2007) TDP1 facilitates repair of ionizing radiation-induced DNA single-strand breaks. *DNA Repair (Amst)*, **6:** 1485–1495

El-Khamisy SF, Saifi GM, Weinfeld M, Johansson F, Helleday T, Lupski JR, Caldecott KW (2005) Defective DNA single-strand break repair in spinocerebellar ataxia with axonal neuropathy-1. *Nature* **434:** 108–113

Hardy RR, Hayakawa K (2001) B cell development pathways. *Annu Rev Immunol* **19:** 595–621

Hatten ME (1985) Neuronal regulation of astroglial morphology and proliferation in vitro. *J Cell Biol* **100:** 384–396

Holm C, Covey JM, Kerrigan D, Pommier Y (1989) Differential requirement of DNA replication for the cytotoxicity of DNA topoisomerase I and II inhibitors in Chinese hamster DC3F cells. *Cancer Res* **49:** 6365–6368

Hsiang YH, Hertzberg R, Hecht S, Liu LF (1985) Camptothecin induces protein-linked DNA breaks via mammalian DNA topoisomerase I. *J Biol Chem* **260:** 14873–14878

Hsiang YH, Lihou MG, Liu LF (1989) Arrest of replication forks by drug-stabilized topoisomerase I-DNA cleavable complexes as a mechanism of cell killing by camptothecin. *Cancer Res* **49:** 5077–5082

Inamdar KV, Pouliot JJ, Zhou T, Lees-Miller SP, Rasouli-Nia A, Povirk LF (2002) Conversion of phosphoglycolate to phosphate termini on 3′ overhangs of DNA double strand breaks by the human tyrosyl-DNA phosphodiesterase hTdp1. *J Biol Chem* **277:** 27162–27168

Interthal H, Chen HJ, Champoux JJ (2005a) Human Tdp1 cleaves a broad spectrum of substrates, including phosphoamide linkages. *J Biol Chem* **280:** 36518–36528

Interthal H, Chen HJ, Kehl-Fie TE, Zotzmann J, Leppard JB, Champoux JJ (2005b) SCAN1 mutant Tdp1 accumulates the enzyme—DNA intermediate and causes camptothecin hypersensitivity. *EMBO J* **24:** 2224–2233

Ismail IH, Nystrom S, Nygren J, Hammarsten O (2005) Activation of ataxia telangiectasia mutated by DNA strand break-inducing agents correlates closely with the number of DNA double strand breaks. *J Biol Chem* **280:** 4649–4655

Kroeger PE, Rowe TC (1989) Interaction of topoisomerase 1 with the transcribed region of the *Drosophila* HSP 70 heat shock gene. *Nucleic Acids Res* **17:** 8495–8509

Lesher DT, Pommier Y, Stewart L, Redinbo MR (2002) 8-Oxoguanine rearranges the active site of human topoisomerase I. *Proc Natl Acad Sci USA* **99:** 12102–12107

Liu C, Pouliot JJ, Nash HA (2002) Repair of topoisomerase I covalent complexes in the absence of the tyrosyl-DNA phosphodiesterase Tdp1. *Proc Natl Acad Sci USA* **99:** 14970–14975

Miao ZH, Agama K, Sordet O, Povirk L, Kohn KW, Pommier Y (2006) Hereditary ataxia SCAN1 cells are defective for the repair of transcription-dependent topoisomerase I cleavage complexes. *DNA Repair (Amst)* **5:** 1489–1494

Nitiss KC, Malik M, He X, White SW, Nitiss JL (2006) Tyrosyl-DNA phosphodiesterase (Tdp1) participates in the repair of Top2-mediated DNA damage. *Proc Natl Acad Sci USA* **103:** 8953–8958

Nivens MC, Felder T, Galloway AH, Pena MM, Pouliot JJ, Spencer HT (2004) Engineered resistance to camptothecin and antifolates by retroviral coexpression of tyrosyl DNA phosphodiesterase-I and thymidylate synthase. *Cancer Chemother Pharmacol* **53:** 107–115

Olive PL, Banath JP, Durand RE (1990) Heterogeneity in radiation-induced DNA damage and repair in tumor and normal cells measured using the 'comet' assay. *Radiat Res* **122:** 86–94

Plo I, Liao ZY, Barcelo JM, Kohlhagen G, Caldecott KW, Weinfeld M, Pommier Y (2003) Association of XRCC1 and tyrosyl DNA phosphodiesterase (Tdp1) for the repair of topoisomerase I-mediated DNA lesions. *DNA Repair (Amst)* **2:** 1087–1100

Pommier Y, Redon C, Rao VA, Seiler JA, Sordet O, Takemura H, Antony S, Meng L, Liao Z, Kohlhagen G, Zhang H, Kohn KW (2003) Repair of and checkpoint response to topoisomerase I-mediated DNA damage. *Mutat Res* **532:** 173–203

Pouliot JJ, Yao KC, Robertson CA, Nash HA (1999) Yeast gene for a Tyr-DNA phosphodiesterase that repairs topoisomerase I complexes. *Science* **286:** 552–555

Pourquier P, Pilon AA, Kohlhagen G, Mazumder A, Sharma A, Pommier Y (1997) Trapping of mammalian topoisomerase I and recombinations induced by damaged DNA containing nicks or gaps. Importance of DNA end phosphorylation and camptothecin effects. *J Biol Chem* **272:** 26441–26447

Pourquier P, Ueng LM, Fertala J, Wang D, Park HJ, Essigmann JM, Bjornsti MA, Pommier Y (1999) Induction of reversible complexes between eukaryotic DNA topoisomerase I and DNA-containing oxidative base damages. 7, 8-dihydro-8-oxoguanine and 5-hydroxycytosine. *J Biol Chem* **274:** 8516–8523

Prise KM, Davies S, Michael BD (1989) Cell killing and DNA damage in Chinese hamster V79 cells treated with hydrogen peroxide. *Int J Radiat Biol* **55:** 583–592

Rodriguez-Galindo C, Radomski K, Stewart CF, Furman W, Santana VM, Houghton PJ (2000) Clinical use of topoisomerase I inhibitors in anticancer treatment. *Med Pediatr Oncol* **35:** 385–402

Rogakou EP, Pilch DR, Orr AH, Ivanova VS, Bonner WM (1998) DNA double-stranded breaks induce histone H2AX phosphorylation on serine 139. *J Biol Chem* **273:** 5858–5868

Rolig RL, McKinnon PJ (2000) Linking DNA damage and neurodegeneration. *Trends Neurosci* **23:** 417–424

Ryan AJ, Squires S, Strutt HL, Johnson RT (1991) Camptothecin cytotoxicity in mammalian cells is associated with the induction of persistent double strand breaks in replicating DNA. *Nucleic Acids Res* **19:** 3295–3300

Strumberg D, Pilon AA, Smith M, Hickey R, Malkas L, Pommier Y (2000) Conversion of topoisomerase I cleavage complexes on the leading strand of ribosomal DNA into 5′-phosphorylated DNA double-strand breaks by replication runoff. *Mol Cell Biol* **20:** 3977–3987

Takashima H, Boerkoel CF, John J, Saifi GM, Salih MA, Armstrong D, Mao Y, Quiocho FA, Roa BB, Nakagawa M, Stockton DW, Lupski JR (2002) Mutation of TDP1, encoding a topoisomerase I-dependent DNA damage repair enzyme, in spinocerebellar ataxia with axonal neuropathy. *Nat Genet* **32:** 267–272

Wang JC (2002) Cellular roles of DNA topoisomerases: a molecular perspective. *Nat Rev Mol Cell Biol* **3:** 430–440

Wood RD, Mitchell M, Lindahl T (2005) Human DNA repair genes, 2005. *Mutat Res* **577:** 275–283

Wu J, Liu LF (1997) Processing of topoisomerase I cleavable complexes into DNA damage by transcription. *Nucleic Acids Res* **25:** 4181–4186

Yang SW, Burgin Jr AB, Huizenga BN, Robertson CA, Yao KC, Nash HA (1996) A eukaryotic enzyme that can disjoin dead-end covalent complexes between DNA and type I topoisomerases. *Proc Natl Acad Sci USA* **93:** 11534–11539

Zhou T, Lee JW, Tatavarthi H, Lupski JR, Valerie K, Povirk LF (2005) Deficiency in 3′-phosphoglycolate processing in human cells with a hereditary mutation in tyrosyl-DNA phosphodiesterase (TDP1). *Nucleic Acids Res* **33:** 289–297